



Article

Rapid and Effective Way to Synthesize Highly Crystalline Nanosized SAPO-34 Particles

Irina Shamanaeva , Svetlana Strelova, Marina Solovyeva and Aleksandra Grekova *

Boriskov Institute of Catalysis SB RAS, Lavrentiev Ave., 5, 630090 Novosibirsk, Russia

* Correspondence: grekova@catalysis.ru

Abstract: SAPO-34 nanocrystals with sizes of 50–150 nm were obtained via steam-assisted crystallization (SAC) for 5 h at 200 °C from two types of aluminum precursors—aluminum isopropoxide and boehmite. A reaction mixture composition with a small amount of organic template tetraethylammonium hydroxide (TEAOH) was used with the molar ratio TEAOH/Al₂O₃ = 1/1. The alumina precursor type and duration of the SAC (5 and 24 h) on the crystal size, texture, and acid properties were investigated. The SAPO-34 nanocrystals that we obtained possess a large micropore volume of 0.22–0.24 cm³/g and a specific surface area of 651–695 m²/g. When the crystallization was prolonged for up to 24 h, a SAPO-18 structure appeared, but the micropore and mesopore volumes changed insignificantly. Using boehmite as the aluminum precursor led to higher mesoporosity of the material but a little bit lower acidity when compared with the samples prepared from aluminum isopropoxide. In addition, the method proposed was used for preparing a SAPO-34-coated aluminum adsorber heat exchanger. Thus, the synthesis method proposed is affordable and effective to prepare SAPO-34 highly crystalline nanoparticles, with no need for post-synthetic procedures as the mother liquor separation from nanocrystals.

Keywords: SAPO-34; dry gel conversion; steam-assisted crystallization; nanocrystals; coated adsorber



Citation: Shamanaeva, I.; Strelova, S.; Solovyeva, M.; Grekova, A. Rapid and Effective Way to Synthesize Highly Crystalline Nanosized SAPO-34 Particles. *Nanomaterials* **2022**, *12*, 4086. <https://doi.org/10.3390/nano12224086>

Received: 31 October 2022

Accepted: 17 November 2022

Published: 20 November 2022

Publisher's Note: MDPI stays neutral with regard to jurisdictional claims in published maps and institutional affiliations.



Copyright: © 2022 by the authors. Licensee MDPI, Basel, Switzerland. This article is an open access article distributed under the terms and conditions of the Creative Commons Attribution (CC BY) license (<https://creativecommons.org/licenses/by/4.0/>).

1. Introduction

Silicoaluminophosphates (SAPOs) are vital members of the molecular sieve family. These zeolite-like materials consist of TO₄-tetrahedra, creating the ordering of the microporous framework, as well as aluminosilicate zeolite, with a difference in the T-atoms (T = Si, Al atoms for the zeolites, and T = Al, P, Si atoms for the SAPOs) [1]. Silicoaluminophosphates are unique materials since the majority of the structures are absent among the aluminosilicate zeolites, although some structures are the same as the aluminosilicate ones; for example, the CHA structure is presented both in AlSi (Chabazite zeolite) and SAPO (SAPO-34) compositions [2]. The framework topology of SAPO-34 is comprised of cylinder-like cages (6.7 × 6.7 × 10.0 Å) with 8-ring pore mouths (3.8 × 3.8 Å), and the small pore mouths only allow linear olefins and small molecules to diffuse through these. SAPO-34 is widely used in catalysis, especially in the catalytic reduction of NO_x [3], methanol-to-olefins (MTO) conversion [4,5], and CO₂ hydrogenation for light olefin production [6,7], as well as in adsorption applications, such as sorbent in adsorption heat pumps [8,9]. The last application is an alternative to conventional electrically driven systems, such as air conditioning, solar air conditioning, waste heat recovery, and domestic heat pumping. However, micrometer-sized crystals have some limitations, e.g., reduced accessibility to acid sites and diffusion restriction because of the long microporous pathways, often resulting in a fast deactivation of zeolite-containing catalysts. The use of nanozeolites can overcome this limitation. Nanozeolites have properties such as enhanced surface areas, high external-to-internal atom number ratios, short diffusion path lengths, accessible active sites, and controllable surface properties, resulting in high activities, better performances, and longer lifetimes [10].

There are several approaches to forming the nanocrystals of zeolites and zeolite-like materials through the control of the crystallization conditions and reaction mixture compositions. Among them are using an extra organic template, controlling the crystallization temperature and duration, and using ultrasonic irradiation, confined-space synthesis in the inert porous matrix, and alternative synthesis approaches, as well as post-synthesis treatment of the primary micrometer-sized zeolites, followed by recrystallization [10–12].

Among the alternative synthesis ways, the dry gel method is particularly worth highlighting [13]. The dry gel crystallization (DGC) approach is divided into two techniques, namely, steam-assisted crystallization (SAC) and vapor-phase transport (VPT).

In the SAC technique, the initial reaction gel containing the organic template is heated to obtain a dried “gel”. Then, the dried gel is placed in autoclaves in a special vessel with a small amount of water at the bottom of the autoclave located separately from the dried gel. In the VPT technique, the organic template is mixed with water and put at the bottom of the autoclave; the dry gel, in turn, does not contain the structure-directing agent. It is believed that the lack of a liquid phase does limit mass transport and, therefore, may result in a lower rate of crystal growth. One of the benefits of using DGC in nanocrystals formation is the no need to separate the nanosized crystals from the mother liquor.

SAPO-34 can also be synthesized by dry gel conversion, especially by SAC. There is a number of papers dedicated to this SAPO-34 synthesis strategy; however, there are only a few revealing SAPO-34 nanocrystal-obtaining. Zhang et al. [14] used diethylamine (DEA) as a structure-directing agent (SDA) in the amount of $\text{DEA}/\text{Al}_2\text{O}_3 = 2/1$ synthesized SAPO-34 crystals of up to 20 μm in size at 200 °C for 5 days, both with the SAC and VPT methods. Rimaz et al. [15] also used DEA with a molar ratio of $\text{DEA}/\text{Al}_2\text{O}_3 = 6/1$, which probably made it possible to reduce the crystallization duration of the steam-assisted conversion to 6–1.5 h. Morpholine (MOR) with $\text{MOR}/\text{Al}_2\text{O}_3 = 4/1$ was used by Askari et al. [16] and Rezaei et al. [17]. In [16], the crystallization duration was reduced for 3–6 h at 200 °C, and SAPO-34 crystals of ca. 0.3–3 μm were obtained. In turn, Rezaei et al. [17] tested an enhanced crystallization temperature of 300–400 °C to form SAPO-34 crystals for 30–45 min, and the SAPO-34 crystals obtained were ca. 0.5–3 μm in size. Zhang et al. [18] also used MOR, but in a VPT conversion, and the synthesis proceeded for 5 days, resulting in large SAPO-34 crystals.

A smaller amount of SDA was used in the SAC by Di et al. [19]. They applied triethylamine (TEA) with a ratio of $\text{TEA}/\text{Al}_2\text{O}_3 = 2.5/1$ to crystallize at 170 °C for 48 h SAPO-34 plate-like nanocrystals using 30 wt.% SAPO-34 seeds, while 5–10 μm cubic crystals were formed without seeds. Finally, tetraethylammonium hydroxide (TEAOH) was used as the SDA in the steam-assisted conversion to form SAPO-34 [20,21]. Chen et al. [20] rather used a combination of the SAC and VPT techniques with varying $\text{TEAOH}/\text{Al}_2\text{O}_3$ ratios from 0.15 to 2 in the reaction mixture and added, additionally, TEA in the bottom of the autoclave and carried out the crystallization at 170 °C for 48 h, obtaining SAPO-34 crystals in the range of sizes 50–500 nm. Hirota et al. [21] crystallized SAPO-34 nanocrystals in the range of 100–150 nm at 180 °C for 1.5–24 h with $\text{TEAOH}/\text{Al}_2\text{O}_3 = 1.8/1$ without additional chemicals or seeds; however, there is no information about the texture properties of the obtained SAPO-34.

SDA mixtures are also used in dry gel conversion to obtain SAPO-34 crystals. Thus, four different templates were used in the amount of $\text{Al}_2\text{O}_3/(\text{TEAOH} + \text{TEA} + \text{MOR} + \text{DEA}) = 1/(0.2 + 0.4 + 0.6 + 0.8)$ and $\text{Al}_2\text{O}_3/(\text{TEAOH} + \text{TEA} + \text{MOR} + \text{DEA}) = 1/(0.4 + 0.2 + 0.8 + 0.6)$ in [22]; these complicated compositions and crystallization conditions (180 °C, 3–8 h) led to large SAPO-34 crystals of 2–10 μm .

Thus, this paper proposes the short-time crystallization method to prepare highly crystalline nanosized particles of SAPO-34 from aluminum isopropoxide or boehmite, with a small amount of organic template TEAOH and without either other additives or SAPO-34 seeds, via the steam-assisted conversion approach.

2. Experimental Section

2.1. Materials and SAPO-34 Synthesis Procedure

Aluminum isopropoxide (AIP, Sigma-Aldrich, St. Louis, MO, USA) or boehmite (84 wt.% Al_2O_3), orthophosphoric acid H_3PO_4 (85%), and fumed SiO_2 (Sigma-Aldrich) were used as the Al, P, and Si sources, respectively. Tetraethylammonium hydroxide (TEAOH, 25 wt.%, Sigma-Aldrich) was the organic structure-directing agent (molecular template).

Silicoaluminophosphates, SAPO-34s, were obtained via the dry gel synthesis approach in accordance with the procedure described below.

Initially, the gel with a molar composition of $1 \text{ Al}_2\text{O}_3/1 \text{ P}_2\text{O}_5/0.3 \text{ SiO}_2/1 \text{ TEAOH}/50 \text{ H}_2\text{O}$ was prepared by the subsequent mixing of the Al source with a H_3PO_4 water solution; then, silica and TEAOH were added to the precursor mixture. The final gel was mixed for 3 h, followed by drying in an oven at $80 \text{ }^\circ\text{C}$ for 24 h to prepare the dry gel. The dry gel that was obtained was homogenized in a mortar. After, this dry gel powder was placed into a small Teflon cup on a Teflon pillar located in the main Teflon vessel in a stainless-steel autoclave. Water was added to the bottom of the main Teflon vessel, separately from the dry gel. A schematic construction of the crystallization vessel is presented in Figure 1. The water/dry gel ratio used was 5 g/3 g. Crystallization was carried out at $200 \text{ }^\circ\text{C}$ for 5 or 24 h. After crystallization, the product was washed with distilled water twice, dried at $100 \text{ }^\circ\text{C}$, and calcined at $600 \text{ }^\circ\text{C}$ for 4 h with a heating rate of $3^\circ/\text{min}$.

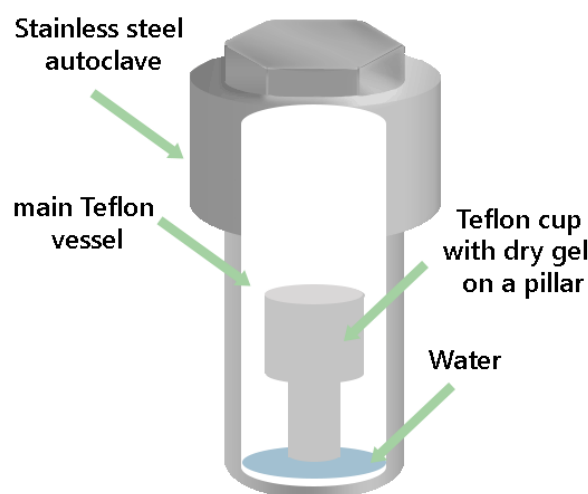


Figure 1. Scheme of a vessel for steam-assisted crystallization.

When AIP was used, the obtained SAPOs were denoted as SAPO-34-5h and SAPO-34-24h, where “5h” and “24h” indicate crystallization time in hours. In the case of the boehmite used as the aluminum source, the sample name has an additional “B”: SAPO-34-B-5h.

2.2. Procedure for Obtaining SAPO-34-Covered Aluminum Heat Exchanger

The fragment of the real aluminum plate-fin heat exchanger (HEX, Yamaha Aerox, Yamaha Corporation, Hamamatsu, Japan) was washed with a citric acid solution in an ultrasonic bath to remove Ca^{2+} and Mg^{2+} salt deposits; then, it was washed with distilled water and dried.

The SAPO-34 precursor mixture was obtained as described above (Al source = AIP) and dried to form a dry gel. To obtain the HEX-supported dry gel, a paste of precursors with a special viscosity was formed with water, adding an approximate ratio of dry gel/water = 1/3. The paste made was applied onto the lamellas of the HEX with subsequent drying at $80 \text{ }^\circ\text{C}$. As a result, the HEX fragment with dry gel inside was obtained. Finally, the HEX-supported dry gel was exposed to steam-assisted crystallization at $200 \text{ }^\circ\text{C}$ for 5 h. After crystallization, the HEX-supported crystallization product was calcined at $600 \text{ }^\circ\text{C}$ to remove the TEAOH molecular template.

2.3. Characterization

The phase composition of the non-calcined samples was determined by X-ray diffraction (XRD) analysis with an ARLX'RA diffractometer with CuK α radiation (wavelength was 1.5418 Å). The crystal morphology and size were studied using scanning electron microscopy (SEM) on a JSM-6460LV (JEOL) operating at an accelerated voltage of 15–20 kV. The acidic properties of SAPOs were analyzed by ammonia temperature-programmed desorption (NH₃-TPD) on a Vra-100 mass spectrometer by an STS instrument in semi-automatic mode. The porous structure of the synthesized samples was studied by low-temperature N₂ adsorption at 77 K on a Quantachrome Nova 1200 gas sorption analyzer. The samples were degassed at 150 °C for 3 h before the N₂ adsorption measurement. The specific surface area, S_{BET}, was calculated using the analysis of the adsorption branch of the isotherm in the relative pressure range of 0.01–0.02, based on the Brunauer–Emmett–Teller theory (BET). The total pore volume, V_{tot}, was calculated from the amount of N₂ adsorbed at a relative pressure of P/P₀ = 0.99. The micropore volume, V_{micro}, was calculated using the statistical thickness analysis of the isotherm adsorption branch and de Boer's t-method. Mesopore distribution was performed based on the Barrett–Joyner–Halenda (BJH) equation and the desorption branch of isotherms. To evaluate the hierarchy of the SAPOs, the hierarchy factor (HF) was estimated using the formula from [23]:

$$HF = (S_{\text{external}}/S_{\text{BET}}) \times (V_{\text{micro}}/V_{\text{tot}}), \text{ where } S_{\text{external}} = S_{\text{BET}} - S_{\text{micro}}$$

IR spectra (64 scans per spectrum, resolution 4 cm⁻¹) were recorded using a Shimadzu IRAffinity-1 spectrometer at 25 °C in the 400 to 4000 cm⁻¹ range. The samples were mixed and ground with KBr (SAPO-34: KBr = 3:97). Thermogravimetric analysis was performed on an automated thermogravimetric analyzer, Discovery TGA 550 (TA Instruments, Inc., New Castle, DE, USA), where the calcined sample (0.070 g) was heated from room temperature to 800 °C at a heating rate of 10 °C/min (Ar flow rate, 60 mL/min). ²⁷Al and ³¹P solid-state NMR spectra were recorded using a Bruker Avance 400 pulsed Fourier spectrometer in a constant magnetic field of 9.4 T, corresponding to the resonant frequencies of 104.31 MHz (²⁷Al) and 161.92 MHz (³¹P). The spectra were recorded at room temperature under 20 kHz magic angle spinning (MAS) conditions with the samples placed inside a standard 2.5 mm ZrO₂ rotor. A non-selective one-pulse excitation was used in the ²⁷Al NMR experiments with the $\pi/6$ pulse length of 0.5 μ s and a 1 s interpulse delay. ³¹P NMR spectra were recorded using a Hahn-echo $\pi/2$ - τ - π sequence with the 2.4 μ s length of a $\pi/2$ pulse and a rotor-synchronized echo delay, τ , of 50 μ s. A 10 s delay between the experiments was used to allow for complete magnetization relaxation. The ²⁷Al spectra were referenced to a 1 M solution of Al(NO₃)₃ at 0 ppm, and the ³¹P NMR spectra were referenced to an 85% H₃PO₄ solution at 0 ppm.

3. Results and Discussion

3.1. SAPO-34 Properties

The XRD patterns (Figure 2) of the samples obtained represent a mainly CHA structure (Figure 2, the grey pattern), and some impurities of the AEI structure (SAPO-18) can be detected at ca. 17° for the SAPO-34–24h sample. It should be noted that reflections of the SAPO-34–5h sample are less intensive than in the case of the other SAPO-34 samples, and that is especially evident for the reflections at 30–32°. When the crystallization time was prolonged from 5 to 24 h, the intensity of some of the reflections was higher, and an AEI structure appeared. The AEI framework consists of layers of double 6-ring units, which are the same as those in the CHA framework. These layers are tilted in the AEI but not in the CHA structure, resulting in a pear-shaped cage with 6 8-membered rings and 12 4-membered rings [24]. The AEI structure competing with the CHA or AEI\CHA intergrowth structures may be observed [25].

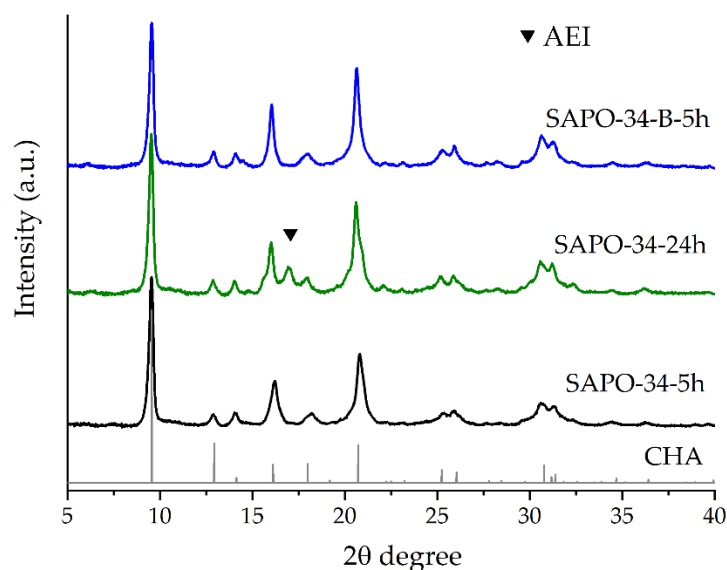


Figure 2. XRD patterns of synthesized SAPO-34. Triangle indicates AEI (SAPO-18) structure.

Meanwhile, the width of the intensities of the SAPO-34-B-5h obtained from boehmite as the aluminum source is similar to the XRD pattern of the SAPO-34-24h obtained from the AIP. Thus, the crystallinity of the SAPO-34 from the boehmite crystallized for 5 h at 200 seems to be close to the SAPO-34 from the AIP crystallized for 24 h.

For a more detailed investigation of the SAPO-34 structure depending on the Al precursor type used, FT-IR spectroscopy, ^{31}P MAS NMR and ^{27}Al MAS NMR spectroscopy, and TGA were carried out for the SAPO-34-5h and SAPO-34-B-5h samples.

The SAPO-34-5h and SAPO-34-B-5h samples are characterized by identical sets of bands in the IR spectra (Figure 3). No bands belonging to the unreacted boehmite were detected in the IR spectrum of SAPO-34-B-5h. Vibration bands at 490 cm^{-1} and 620 cm^{-1} are ascribed to the Si-O bending of the SiO_4 tetrahedral and the T-O (T = Si, Al, P) bending in the double-6 rings, respectively. The absorption peaks at 700 cm^{-1} and the broad-band at $1000\text{--}1250\text{ cm}^{-1}$ are associated with the symmetric stretching vibration of T-O and the asymmetric stretching vibration of T-O-T (Al-O-Si, Si-O-Si, and P-O-Al), respectively. The intensive band at 1650 cm^{-1} is attributed to the vibrations of physically adsorbed water molecules [26].

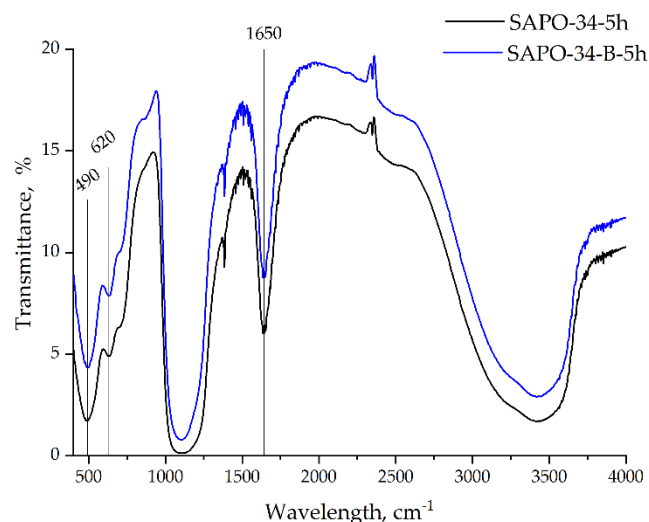


Figure 3. FT-IR spectra of SAPO-34 samples synthesized from AIP (SAPO-34-5h) and boehmite (SAPO-34-B-5h).

Finally, a broad band in the range of 3000–3700 cm^{-1} is attributed to hydroxyl groups, such as P-OH, Al-OH, Si-OH, and the bridging Si-O(OH)-Al [27].

The obtained ^{27}Al and ^{31}P MAS NMR spectra (Figure 4) fully correspond to the spectra reported for hydrated SAPO-34 [28]. The ^{31}P NMR spectra of both samples are identical within the experimental error and contain a dominating line at -27 ppm that corresponds to the framework $\text{P}(\text{OAl})_4$ sites and a broad shoulder stretching from -10 to -20 ppm that corresponds to hydrated phosphorus sites. The ^{27}Al NMR spectra contain three distinct lines that correspond to tetrahedrally (39 ppm), pentahedrally (14 ppm), and octahedrally (-13 ppm) coordinated Al sites. The framework alumina sites are silicoalumophosphates and possess a tetrahedral coordination, while the sites with a higher coordination arise from the presence of one or two additional water molecules in their local environment. The relative line intensities of the studied sample differ slightly with the presence of a larger amount of octahedrally coordinated sites in the SAPO-34-B-5h sample. At the same time, the amount of 5-coordinated Al sites is slightly higher in the SAPO-34-5h sample.

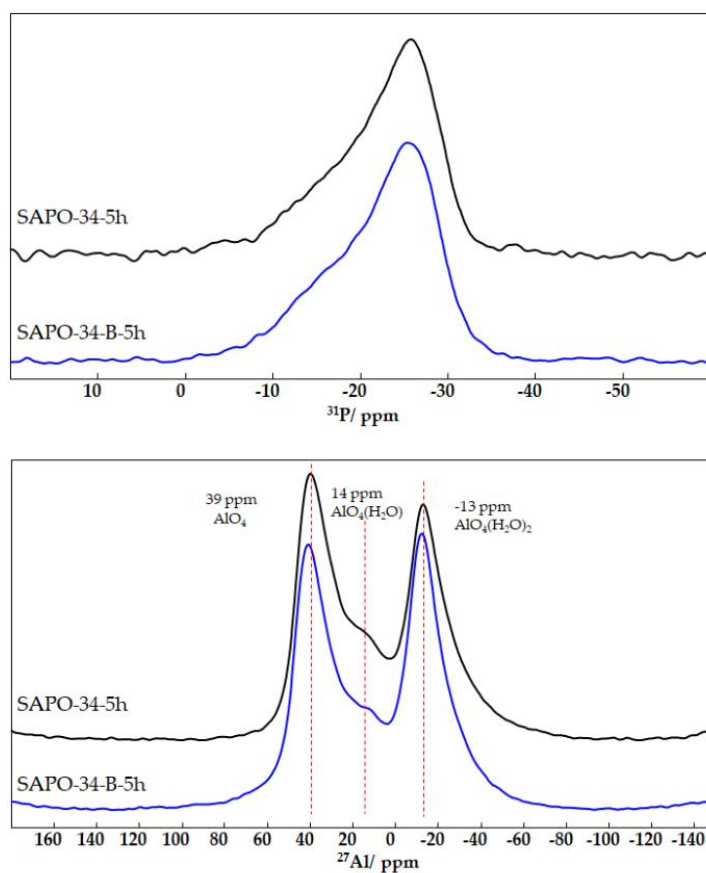


Figure 4. ^{31}P (top) and ^{27}Al (down) NMR spectra of SAPO-34 samples synthesized from AIP (SAPO-34-5h) and boehmite (SAPO-34-B-5h).

The TGA profiles (Figure 5) of the calcined SAPO-34-5h and SAPO-34-B-5h samples show one weight loss at the temperature of up to 230 $^{\circ}\text{C}$ related to water desorption. The weight loss is larger in the case of the SAPO-34-B-5h sample that corresponds to the ^{27}Al NMR data (more Al atoms coordinated with an additional two H_2O molecules).

Thus, regardless of the Al precursor (AIP or boehmite), the structure of SAPO-34 is similar to each other, and only the adsorbed water amount is bigger in the case of SAPO-34-B-5h, which may be a result of a larger pore volume.

Figure 6 represents the SEM images of the obtained samples. All of the samples are nanocrystals. SAPO-34-5h (Figure 6a,b) consists of ca. 100 nm plate-like nanocrystals with sizes up to 800 nm. SAPO-34-24h (Figure 6c,d) represents mostly nano-plate crystals,

while the SAPO-18 crystals are difficult to detect. The boehmite precursor led to more isometric nanocrystals of SAPO-34-B-5h. According to the images of the scanning electron microscopy, the SAPO-34 crystals, which were formed for 5 h, of the DGC are smaller in the case of using AIP than boehmite.

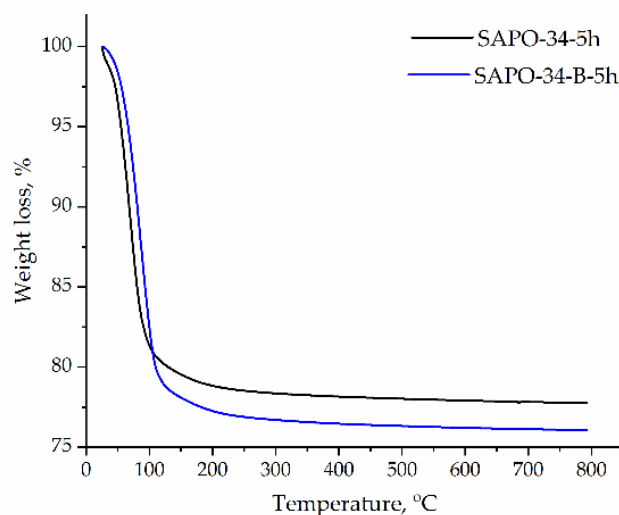


Figure 5. TG analysis of SAPO-34 samples synthesized from AIP (SAPO-34–5h) and boehmite (SAPO-34–B–5h).

Thus, dry gel crystallization for 5 h at 200 °C led to SAPO-34 nanocrystals, regardless of the aluminum precursor type, in this work. Only morphology differences can be identified.

Figure 7a represents N₂ adsorption-desorption isotherms of the obtained samples. All of the isotherms are of the IV type, which characterizes micro-mesoporous materials. At P/P₀ > 0.4, the capillary condensation of nitrogen arises, and the hysteresis loop of the H4 type is observed. This type of hysteresis loop describes the presence of aggregates of crystals with pores of different shapes and sizes. The larger hysteresis loop of SAPO-34–B–5h means a higher mesopore volume of the sample among all the samples in this work. Indeed, according to the BJH pore size distribution (Figure 7b), sample SAPO-34–B–5h exhibits high values of differential pore volume (dV/logD).

Additionally, the pore size distribution for the SAPO-34 samples (Figure 7b) showed distinct maxima at 3.7 nm, which is also observed in other zeolite and zeolite-like materials [29–31] and is attributed to the tensile strength effect of the adsorbed phase [32]. A broad distribution from 10 to 100 nm is centered at about 40 nm, representing the intercrystalline mesopores in the SAPO-34.

Table 1 shows the quantitative texture parameters of the silicoaluminophosphates. Interestingly, the micropore volume is almost the same for all of the SAPO-34 samples and amounts to 0.22–0.24 cm³/g; the microporosity of the SAPO-34, obtained from either the AIP or boehmite, crystallized for 5 h and is similar to each other and, apparently, slightly depends on the alumina precursor, as well as the crystallization duration, when DGC was used at the given crystallization conditions and molar composition.

Table 1. Texture properties of SAPO-34.

Sample	S _{BET} , m ² /g	S _{external} , m ² /g	V _{micro} , cm ³ /g	V _{meso} , cm ³ /g	HF
SAPO-34-5h	651	68	0.22	0.29	0.045
SAPO-34-24h	695	52	0.24	0.32	0.032
SAPO-34-B-5h	668	57	0.23	0.46	0.028

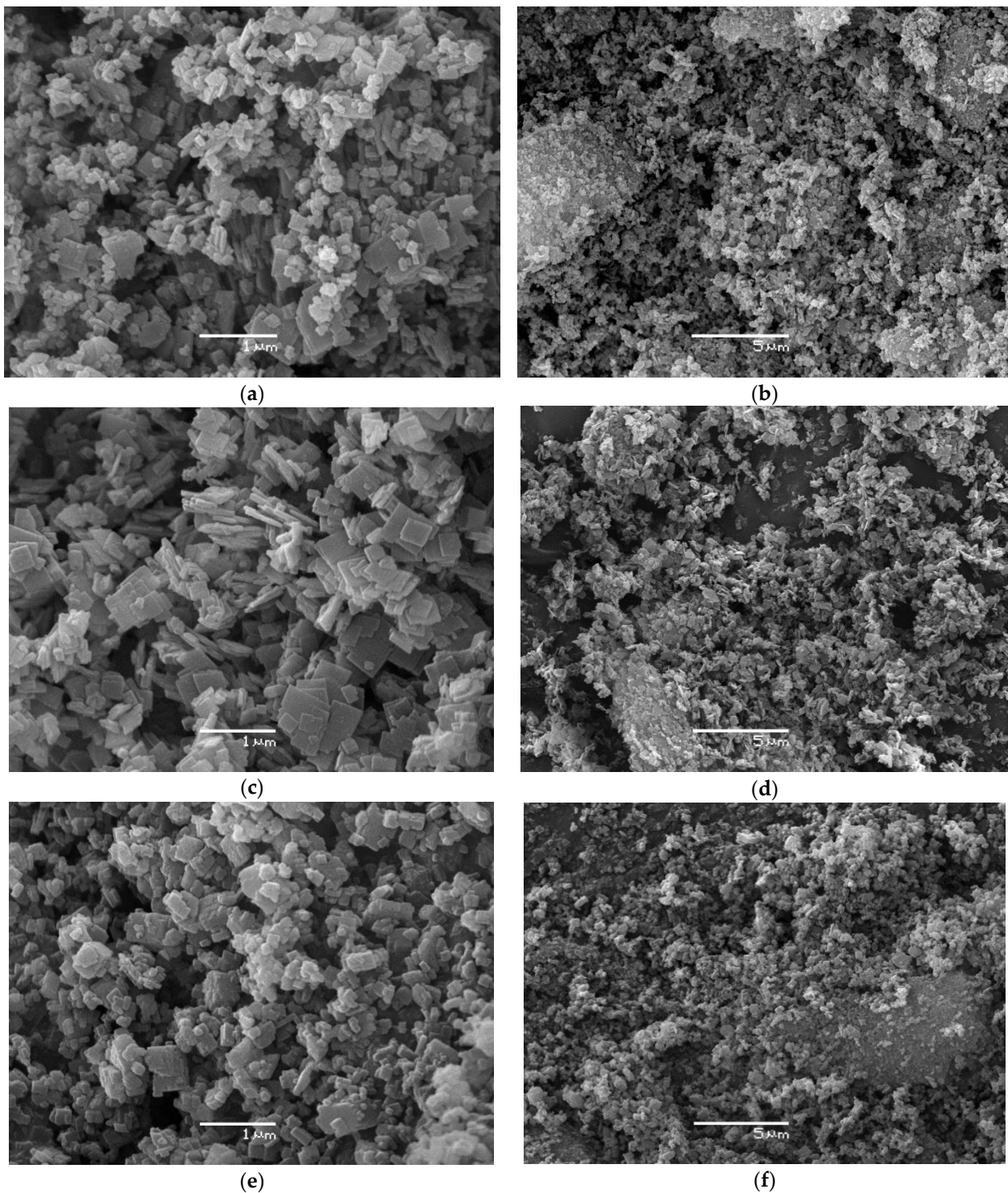


Figure 6. SEM images of SAPO-34 crystals: (a,b) SAPO-34-5h; (c,d) SAPO-34-24h; (e,f) SAPO-34-B-5h.

Notably, the mesoporosity of the SAPO-34 samples crystallized with AIP as the aluminum source is very similar, provided that crystallization proceeded for a different time (0.29 and 0.32 cm³/g). Moreover, even though the crystals of the SAPO-34-5h sample are smaller than those of SAPO-34-B-5h visually (Figure 6a,e), the first is less mesoporous (0.29 vs. 0.46 cm³/g).

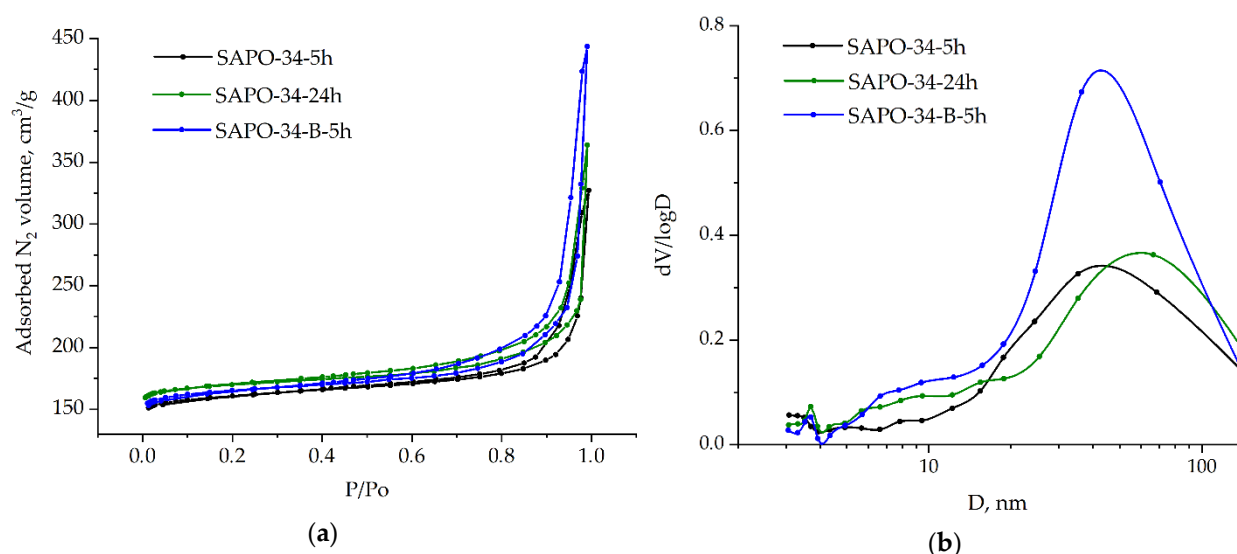


Figure 7. (a) Nitrogen sorption isotherms; (b) BJH pore size distribution of obtained SAPO-34.

Assembling the nanocrystals is one of the ways to design hierarchical zeolites. Zeolites of this type have additional meso- and/or macro-pores. Micro- and meso-pores of uniform size are responsible for the size and shape selectivity of guest molecules and improving interactions between the host and guest molecules, whereas large meso- and macro-pores promote molecular diffusion and accessibility to the active sites. It is believed that meso-pores in a hierarchical zeolite can be present mainly in two forms: intercrystalline and intracrystalline [33]. A hierarchical zeolite with an intercrystalline mesoporous structure can be obtained by controlling the conditions to reinforce the nucleation, nanozeolite preparation, and aggregation of nanozeolite seeds with voids between them [10].

To estimate the hierarchy of the nanocrystal samples of SAPO-34, the HF was calculated for the synthesized silicoaluminophosphates. The HF is a useful tool to compare the textural properties of zeolites, showing the balance between the external surface of the sample and the volume of the micropores. It turned out that, in spite of the large mesopore volume (57–67% of the total pore volume), the HF indicates the absence of hierarchical porosity, and for all of the samples obtained in this work, the HF is in the range of 0.028–0.045 (Table 1). Thus, as shown in [23], the range of $0.05 < HF < 0.1$ is typical, and $HF > 0.15$ is for zeolites with an intracrystalline mesoporosity formed by leaching.

Hence, the HF is less than 0.05 because the small external surface area that pointed to the nanocrystals is not highly aggregated together. However, nanocrystals are able to reduce the mass transport limitations due to the shortest diffusion path in the micropore space [11].

In general, according to texture data (Table 1), all of the samples possess a large, specific surface area in the range of 650–695 m²/g and are highly micro-mesoporous silicoaluminophosphates.

The ammonia TPD curves of SAPO-34-5h and SAPO-34-24h are similar enough (Figure 8). The total amount of NH₃ desorbed is 1.37 mmol/g and 1.41 mmol/g, respectively. At the same time, the difference in the total ammonia desorbed between the SAPO-34 crystallized for 5 h when AIP or boehmite used as the Al precursor is 14.5% (1.37 and 1.17 mmol/g, respectively). Taking into account the same silicon content in the initial gel and the dry gel synthesis approach used, which excepts the mother liquor, it can be supposed that the Si content in all of the SAPO-34s is similar. Thus, the difference in the acidity of the SAPO-34 synthesized from the AIP and boehmite may be caused by the specific Si location in the SAPO framework due to a different contribution of the SM2 and SM3 mechanisms [34].

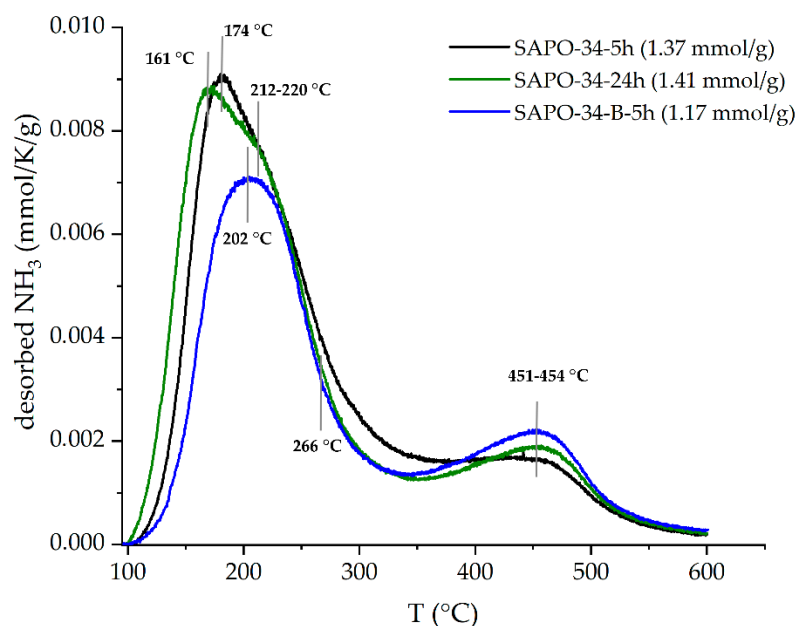


Figure 8. Ammonia TPD curves of SAPO-34.

The TPD curve of the SAPO-34 crystallized from boehmite differs from other ones of the SAPO-34 obtained from the AIP-contained precursor mixture in the temperature of NH_3 desorption; this shift to a higher temperature indicates stronger acid sites in SAPO-34-B-5h. First, the desorption peak is at a temperature of 202 °C vs. 161–174 °C for the other SAPO-34; the second hidden peak (the shoulder) shifts from 212–220 °C to 266 °C, and the third one is detected at around 451–454 °C for all of the SAPO-34s. The low-temperature desorption peaks are attributed to the physical adsorption of NH_3 at weak acidic sites, indicating the presence of Si–OH, P–OH, and Al–OH; the peaks at high-temperature desorption of NH_3 indicate strong Brønsted acid sites, formed by the hydroxyl groups of Si–OH–Al.

Table 2 shows the total amount of desorbed ammonia (n , the acid site density) and individual desorption maximum.

Table 2. Acid properties of SAPO-34.

Sample	$n \text{ NH}_3$ (161–202 °C), mmol/g	$n \text{ NH}_3$ (212–266 °C), mmol/g	$n \text{ NH}_3$ (451–454 °C), mmol/g	Total Amount, mmol/g
SAPO-34-5h	0.29	0.64	0.44	1.37
SAPO-34-24h	0.27	0.77	0.37	1.41
SAPO-34-B-5h	0.60	0.24	0.33	1.17

Noteworthy, the SAPO-34 synthesized with molar $\text{TEAOH}/\text{Al}_2\text{O}_3/\text{SiO}_2 = 1/1/0.6$ in [4] possessed two times less acidity than the SAPO-34 in this work, provided that there was two times bigger initial SiO_2 content.

3.2. Primary Experiments on Obtaining Aluminum Heat Exchanger Covered by SAPO-34

The method proposed has been tested to obtain primary experimental samples of the aluminum heat exchanger (HEX) fragment covered by SAPO-34 crystals for water sorption.

The simplest way to apply adsorbents is by placing loose granules inside the heat exchanger (AdHEX) [35]; however, different ways to coat it are developing, such as by direct crystallization and the dip-coating approach [35,36]. Intensification of the heat flow from the adsorbent to the heat transfer liquid has been marked as a key challenge in recent years [37,38]. One of the promising ways here was to switch from a granular bed adsorber to coating the adsorbent directly onto the heat exchanger [39]. Dip-coating implies using a

binder, which reduces the adsorption capacity by 10–20% due to decreasing the surface area and the pore volume. Moreover, using additional chemicals is required [40].

There are several papers devoted to the direct synthesis of SAPO-34 on supports. Bonaccorsi et al. conducted SAPO-34 synthesis on stainless-steel and aluminum supports (rectangular pieces) [41] at 200 °C for 72 h, as well as on aluminum foam [42].

In this work, the fragment of the initial uncovered aluminum HEX is presented in Figure 9a. After the first experiments on the in situ crystallization of the SAPO-34 via the steam-assisted approach at 200 °C for 5 h, the aluminum HEX sample was not destroyed and corroded, and white coatings of the SAPO-34 inside the HEX were observed (Figure 9b). The covering takes place through all of the lamellas, which could be seen when the HEX fragment was dissected (Figure 9c).

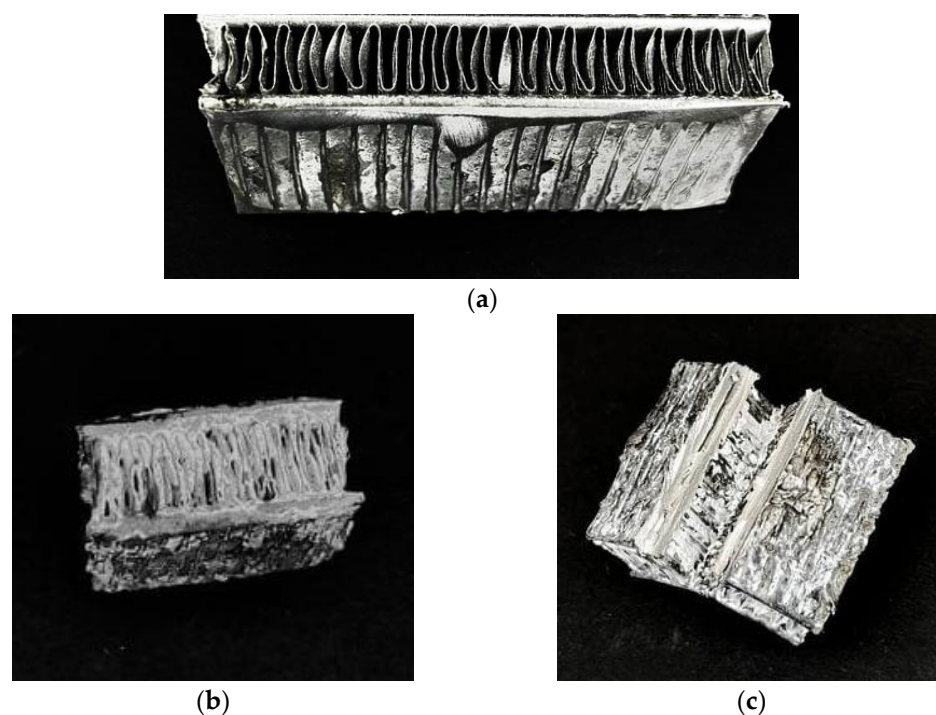


Figure 9. Photographs of part of (a) the uncovered aluminum heat exchanger; (b) the aluminum heat exchanger covered by SAPO-34 obtained via DGC, top view; (c) the aluminum heat exchanger covered by SAPO-34 obtained via SAC, dissected view.

According to the XRD analysis (not given) of powder scraped off, the XRD pattern is similar to the SAPO-34–5h sample and presents SAPO-34.

Thus, the principal possibility of the in situ preparation of a SAPO-34-covered AdHEX via the rapid SAC method has been shown. Further, this method to obtain a covered adsorber heat exchanger will be developed to obtain uniform coverage with a certain thickness and improved mechanical properties with subsequent water vapor adsorption measurements, compared with the granulated AdHEX.

4. Conclusions

SAPO-34 nanocrystals with sizes of 50–150 nm were obtained via the dry gel conversion approach, namely by steam-assisted crystallization for a very short time (5 h) at 200 °C. The crystals obtained are highly crystalline with large micro-pore volumes and specific surface areas (0.22–0.24 cm³/g and 651–695 m²/g, respectively). Meanwhile, a simple reaction mixture composition with a small amount of an organic template was used. We showed that crystallization prolongation from 5 to 24 h causes an AEI (SAPO-18) structure appearance, and the micro-pore and meso-pore volumes change insignificantly. Using boehmite as the aluminum precursor led to a higher mesoporosity of the material but a

little bit lower acidity compared with the samples prepared from aluminum isopropoxide. The primary experiments on obtaining the adsorber heat exchanger via the rapid method proposed were made, and this approach to obtaining heat exchangers coated with SAPO-34 is going to be developed.

Thus, the synthesis method proposed is affordable and effective for preparing highly crystalline nanoparticles of SAPO-34 with no need for post-synthetic procedures as the mother liquor separation from nanocrystals. The method also can be used to make coated adsorber heat exchangers.

Author Contributions: Conceptualization, I.S. and A.G.; methodology, I.S.; validation, A.G.; formal analysis, I.S., S.S. and M.S.; investigation, I.S., S.S. and M.S.; resources, A.G.; data curation, I.S., S.S. and M.S.; writing—original draft preparation, I.S., S.S. and M.S.; writing—review and editing, I.S. and A.G.; visualization, I.S., S.S. and M.S.; supervision, A.G.; project administration, A.G.; funding acquisition, A.G. All authors have read and agreed to the published version of the manuscript.

Funding: The work was supported by the Russian Science Foundation (grant No. 21-79-10183).

Data Availability Statement: Data are available on request from the corresponding author.

Acknowledgments: The authors are grateful to Alekseeva N.A. (XRD patterns), Rudina N.A. (the obtained SEM images), Vdovichenko V.A. (NH₃-TPD measurement), and Yakovlev I.V. (MAS NMR spectra).

Conflicts of Interest: The authors declare no conflict of interest.

Abbreviations

AdHEX	Adsorber heat exchanger
AEI	Aluminum phosphate—Eighteen (International Zeolite Association code)
AIP	Aluminum isopropoxide
BET	Brunauer–Emmett–Teller theory
BJH	Barrett–Joyner–Halenda
CHA	Chabazite
DEA	Diethylamine
DGC	Dry gel conversion
HEX	Heat exchanger
HF	Hierarchy factor
MOR	Morpholine
MTO	Methanol-to-olefins
NH ₃ -TPD	ammonia temperature-programmed desorption
SAC	Steam-assisted crystallization
SAPO	Silicoaluminophosphate(s)
SDA	Structure-directing agent
SEM	Scanning electron microscopy
TEA	Triethylamine
TEAOH	Tetraethylammonium hydroxide
VPT	Vapor-phase transport
XRD	X-ray diffraction

References

1. Flanigen, E.M.; Lok, B.M.; Patton, R.L.; Wilson, S.T. Aluminophosphate Molecular Sieves and the Periodic Table. *Stud. Surf. Sci. Catal.* **1986**, *28*, 103–112.
2. Baerlocher, C.; McCusker, L.B.; Olson, D.H. *Atlas of Zeolite Framework Types*, 6th ed.; Elsevier: Amsterdam, The Netherlands, 2007; ISBN 978-0-444-53064-6.
3. Jabłońska, M. Recent Progress in the Selective Catalytic Reduction of NO with NH₃ on Cu-SAPO-34 Catalysts. *Mol. Catal.* **2022**, *518*, 112111–112133. [[CrossRef](#)]
4. Shamanaeva, I.A.; Yu, Z.; Utemov, A.V.; Wu, W.; Sladkovskiy, D.A.; Parkhomchuk, E.V. Role of Texture and Acidity of SAPO-34 in Methanol to Olefins Conversion. *Pet. Chem.* **2020**, *60*, 471–478. [[CrossRef](#)]
5. Tian, P.; Wei, Y.; Ye, M.; Liu, Z. Methanol to Olefins (MTO): From Fundamentals to Commercialization. *ACS Catal.* **2015**, *5*, 1922–1938. [[CrossRef](#)]

6. Zhang, W.; Wang, S.; Guo, S.; Qin, Z.; Dong, M.; Wang, J.; Fan, W. Effective Conversion of CO₂ into Light Olefins along with Generation of Low Amounts of CO. *J. Catal.* **2022**, *413*, 923–933. [[CrossRef](#)]
7. Li, W.; Wang, H.; Jiang, X.; Zhu, J.; Liu, Z.; Guo, X.; Song, C. A Short Review of Recent Advances in CO₂ Hydrogenation to Hydrocarbons over Heterogeneous Catalysts. *RSC Adv.* **2018**, *8*, 7651–7669. [[CrossRef](#)]
8. Calabrese, L.; Bonaccorsi, L.; Bruzzaniti, P.; Proverbio, E.; Freni, A. SAPO-34 Based Zeolite Coatings for Adsorption Heat Pumps. *Energy* **2019**, *187*, 115981–115988. [[CrossRef](#)]
9. Zheng, X.; Wang, R.Z.; Ge, T.S.; Hu, L.M. Performance Study of SAPO-34 and FAPO-34 Desiccants for Desiccant Coated Heat Exchanger Systems. *Energy* **2015**, *93*, 88–94. [[CrossRef](#)]
10. Koohsaryan, E.; Anbia, M. Nanosized and Hierarchical Zeolites: A Short Review. *Chin. J. Catal.* **2016**, *37*, 447–467. [[CrossRef](#)]
11. Tosheva, L.; Valtchev, V.P. Nanozeolites: Synthesis, Crystallization Mechanism, and Applications. *Chem. Mater.* **2005**, *17*, 2494–2513. [[CrossRef](#)]
12. Askari, S.; Siahmard, A.B.; Halladj, R.; Alipour, S.M. Different Techniques and Their Effective Parameters in Nano SAPO-34 Synthesis: A Review. *Powder Technol.* **2016**, *301*, 268–287. [[CrossRef](#)]
13. Yu, W.; Wu, X.; Cheng, B.; Tao, T.; Min, X.; Mi, R.; Huang, Z.; Fang, M.; Liu, Y. Synthesis and Applications of SAPO-34 Molecular Sieves. *Chem. Eur. J.* **2022**, *28*, e202102787. [[PubMed](#)]
14. Zhang, L.; Bates, J.; Chen, D.; Nie, H.Y.; Huang, Y. Investigations of Formation of Molecular Sieve SAPO-34. *J. Phys. Chem. C* **2011**, *115*, 22309–22319. [[CrossRef](#)]
15. Rimaz, S.; Halladj, R.; Askari, S. Synthesis of Hierarchical SAPO-34 Nano Catalyst with Dry Gel Conversion Method in the Presence of Carbon Nanotubes as a Hard Template. *J. Colloid Interface Sci.* **2016**, *464*, 137–146. [[CrossRef](#)] [[PubMed](#)]
16. Askari, S.; Sedighi, Z.; Halladj, R. Rapid Synthesis of SAPO-34 Nanocatalyst by Dry Gel Conversion Method Templated with Morpholine: Investigating the Effects of Experimental Parameters. *Microporous Mesoporous Mater.* **2014**, *197*, 229–236. [[CrossRef](#)]
17. Rezaei, Y.; Halladj, R.; Askari, S.; Tarjomannejad, A.; Rezaei, T. High-Temperature Synthesis of SAPO-34 Molecular Sieve Using a Dry Gel Method. *Particuology* **2016**, *27*, 61–65. [[CrossRef](#)]
18. Zhang, L.; Huang, Y. Crystallization and Catalytic Properties of Molecular Sieve SAPO-34 by a Vapor-Phase Transport Method. *J. Mater. Chem. A* **2015**, *3*, 4522–4529. [[CrossRef](#)]
19. Di, C.Y.; Li, X.F.; Wang, P.; Li, Z.H.; Fan, B.B.; Dou, T. Green and Efficient Dry Gel Conversion Synthesis of SAPO-34 Catalyst with Plate-like Morphology. *Pet. Sci.* **2017**, *14*, 203–213. [[CrossRef](#)]
20. Li, Z.H.; Li, X.F.; Di, C.Y.; Dou, T.; Chen, S.L. A Green and Cost-Effective Synthesis of Hierarchical SAPO-34 through Dry Gel Conversion and Its Performance in a Methanol-to-Olefin Reaction. *Ind. Eng. Chem. Res.* **2021**, *60*, 15380–15390. [[CrossRef](#)]
21. Hirota, Y.; Murata, K.; Tanaka, S.; Nishiyama, N.; Egashira, Y.; Ueyama, K. Dry Gel Conversion Synthesis of SAPO-34 Nanocrystals. *Mater. Chem. Phys.* **2010**, *123*, 507–509. [[CrossRef](#)]
22. Riyar, B.K.; Agarwal, V.K. Synthesis of SAPO-34 Using the Different Combinations of Four Templates by Dry Gel Conversion Method. *Braz. J. Chem. Eng.* **2021**, *38*, 887–900. [[CrossRef](#)]
23. Pérez-Ramírez, J.; Verboekend, D.; Bonilla, A.; Abelló, S. Zeolite Catalysts with Tunable Hierarchy Factor by Pore-Growth Moderators. *Adv. Funct. Mater.* **2009**, *19*, 3972–3979. [[CrossRef](#)]
24. Poulet, G.; Tuel, A.; Sautet, P. A Combined Experimental and Theoretical Evaluation of the Structure of Hydrated Microporous Aluminophosphate AlPO₄-18. *J. Phys. Chem. B* **2005**, *109*, 22939–22946. [[CrossRef](#)] [[PubMed](#)]
25. Wang, Y.; Chen, S.L.; Jiang, Y.J.; Cao, Y.Q.; Chen, F.; Chang, W.K.; Gao, Y.L. Influence of Template Content on Selective Synthesis of SAPO-18, SAPO-18/34 Intergrowth and SAPO-34 Molecular Sieves Used for Methanol-to-Olefins Process. *RSC Adv.* **2016**, *6*, 104985–104994. [[CrossRef](#)]
26. Zhao, D.; Zhang, Y.; Li, Z.; Wang, Y.; Yu, J. Synthesis of SAPO-18/34 Intergrowth Zeolites and Their Enhanced Stability for Dimethyl Ether to Olefins. *RSC Adv.* **2017**, *7*, 939–946. [[CrossRef](#)]
27. Izadbakhsh, A.; Farhadi, F.; Khorasheh, F.; Sahebdehfar, S.; Asadi, M.; Feng, Y.Z. Effect of SAPO-34's Composition on Its Physico-Chemical Properties and Deactivation in MTO Process. *Appl. Catal. A Gen.* **2009**, *364*, 48–56. [[CrossRef](#)]
28. Buchholz, A.; Wang, W.; Xu, M.; Arnold, A.; Hunger, M. Thermal Stability and Dehydroxylation of Brønsted Acid Sites in Silicoaluminophosphates H-SAPO-11, H-SAPO-18, H-SAPO-31, and H-SAPO-34 Investigated by Multi-Nuclear Solid-State NMR Spectroscopy. *Microporous Mesoporous Mater.* **2002**, *56*, 267–278. [[CrossRef](#)]
29. Danilina, N.; Krumeich, F.; Van Bokhoven, J.A. Hierarchical SAPO-5 Catalysts Active in Acid-Catalyzed Reactions. *J. Catal.* **2010**, *272*, 37–43. [[CrossRef](#)]
30. Guo, L.; Bao, X.; Fan, Y.; Shi, G.; Liu, H.; Bai, D. Impact of Cationic Surfactant Chain Length during SAPO-11 Molecular Sieve Synthesis on Structure, Acidity, and n-Octane Isomerization to Di-Methyl Hexanes. *J. Catal.* **2012**, *294*, 161–170. [[CrossRef](#)]
31. Li, X.; Rezaei, F.; Ludlow, D.K.; Rownaghi, A.A. Synthesis of SAPO-34@ZSM-5 and SAPO-34@Silicalite-1 Core-Shell Zeolite Composites for Ethanol Dehydration. *Ind. Eng. Chem. Res.* **2018**, *57*, 1446–1453. [[CrossRef](#)]
32. Groen, J.C.; Peffer, L.A.A.; Pérez-Ramírez, J. Pore Size Determination in Modified Micro- and Mesoporous Materials. Pitfalls and Limitations in Gas Adsorption Data Analysis. *Microporous Mesoporous Mater.* **2003**, *60*, 1–17. [[CrossRef](#)]
33. Schwieger, W.; Machoke, A.G.; Weissenberger, T.; Inayat, A.; Selvam, T.; Klumpp, M.; Inayat, A. Hierarchy Concepts: Classification and Preparation Strategies for Zeolite Containing Materials with Hierarchical Porosity. *Chem. Soc. Rev.* **2016**, *45*, 3353–3376. [[CrossRef](#)] [[PubMed](#)]

34. Sastre, G.; Lewis, D.; Catlow, C. Mechanisms of silicon incorporation in aluminophosphate molecular sieves. *J. Mol. Catal. A Chem.* **1997**, *119*, 349–356. [[CrossRef](#)]
35. Freni, A.; Bonaccorsi, L.; Calabrese, L.; Capri, A.; Frazzica, A.; Sapienza, A. SAPO-34 coated adsorbent heat exchanger for adsorption chillers. *Appl. Therm. Eng.* **2015**, *82*, 1–7. [[CrossRef](#)]
36. Freni, A.; Frazzica, A.; Dawoud, B.; Chmielewski, S.; Calabrese, L.; Bonaccorsi, L. Adsorbent coatings for heat pumping applications: Verification of hydrothermal and mechanical stabilities. *Appl. Therm. Eng.* **2013**, *50*, 1658–1663. [[CrossRef](#)]
37. Lang, R.; Roth, M.; Stricker, M.; Westerfeld, T. Development of a modular zeolite-water heat pump. *Heat Mass Transf.* **1999**, *35*, 229–234. [[CrossRef](#)]
38. Restuccia, G. Zeolite heat pump for domestic heating. *Energy* **1988**, *13*, 333–342. [[CrossRef](#)]
39. Tatlier, M.; Erdem-Şenatalar, A. Optimization of the cycle durations of adsorption heat pumps employing zeolite coatings synthesized on metal supports. *Microporous Mesoporous Mater.* **2000**, *34*, 23–30. [[CrossRef](#)]
40. Feng, C.; E, J.; Han, W.; Deng, Y.; Zhang, B.; Zhao, X.; Han, D. Key technology and application analysis of zeolite adsorption for energy storage and heat-mass transfer process: A review. *Renew. Sustain. Energy Rev.* **2021**, *144*, 110954–110981. [[CrossRef](#)]
41. Bonaccorsi, L.; Calabrese, L.; Freni, A.; Proverbio, E.; Restuccia, G. Zeolites direct synthesis on heat exchangers for adsorption heat pumps. *Appl. Therm. Eng.* **2013**, *50*, 1590–1595. [[CrossRef](#)]
42. Bonaccorsi, L.; Calabrese, L.; Freni, A.; Proverbio, E. Hydrothermal and microwave synthesis of SAPO (CHA) zeolites on aluminium foams for heat pumping applications. *Microporous Mesoporous Mater.* **2013**, *167*, 30–37. [[CrossRef](#)]